Constitutive Androstane Receptor induces Ribonucleotide Reductase-M2 expression and maintains hepatocyte ploidy in mice

Anjana Asokakumar[1*], Bhoomika Mathur[1*], Sandip Chorghade[2], Anthony Chau[1], Bea Cronologia[1], Frances Alencastro[3], Linda Wheeler[4], Christopher K. Mathews[4], David D. Moore[5], Andrew W. Duncan[3], and Sayeepriyadarshini Anakk[1, 6, 7, §]

[1]Department of Molecular and Integrative Physiology, University of Illinois at Urbana-Champaign, Champaign, IL, USA, [2]Department of Biochemistry, University of Illinois at Urbana-Champaign, Champaign, IL, USA, [3]Department of Pathology, Pittsburgh Liver Research Center, University of Pittsburgh, Pittsburgh, Pennsylvania, USA, [4]Department of Biochemistry and Biophysics, Oregon State University, Oregon, USA, [5]Nutritional Science and Toxicology, University of California, Berkeley, USA, [6]Division of Nutritional Sciences, [7]Cancer Center at Illinois, University of Illinois at Urbana-Champaign, Champaign, IL,, USA.

*Co-first authors, [§]Corresponding author: anakk@illinois.edu

Abstract

The nuclear receptor Constitutive Androstane Receptor (CAR/NR1i3) is known for regulating various liver functions, including detoxification, nutrient metabolism, and hepatocyte proliferation. While CAR activation has been previously linked to higher ploidy, the underlying mechanisms are not fully known. Here, we uncover a basal role for CAR in maintaining hepatocyte ploidy, such that CAR deletion increases the number of diploid (2c) hepatocytes with a concomitant reduction in tetraploid (4c) hepatocytes. We demonstrate that CAR controls the *de novo* dNTP synthesis by directly transactivating the Ribonucleotide Reductase-M2 (*RRM2*) gene, which encodes the rate-limiting catalytic subunit of the enzyme, ribonucleotide reductase. Further, we find that the ligand-dependent CAR activation is sufficient to induce several genes involved in the *de novo* dNTP synthesis pathways, resulting in higher hepatic dATP and dTTP levels within the liver. Importantly, overexpressing RRM2 levels in CAR knockouts led to increased DNA synthesis and tetraploid (4c) hepatocytes compared to the control mice. Importantly, we demonstrate that CAR-mediated DNA synthesis in liver cells is dependent on catalytically active RRM2 function. Taken together, these findings reveal that the CAR-mediated RRM2 regulation contributes towards DNA synthesis and thereby maintains hepatocyte ploidy.

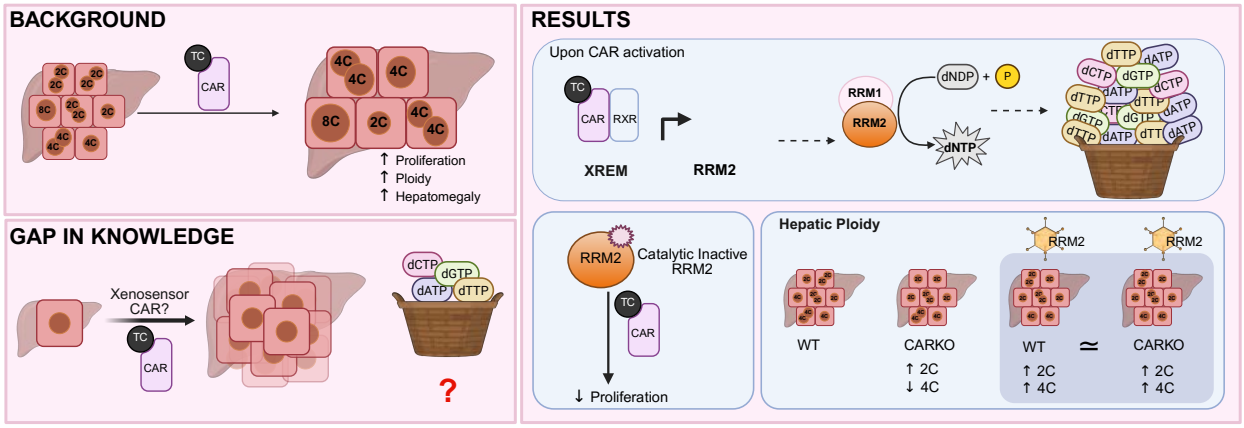

35 **Introduction**

36 The liver is a metabolic hub and is responsible for many cellular functions(1, 2).
37 Hepatocytes carry out detoxification and intermediary metabolism and comprise 70-80% of the
38 liver tissue(3–5). A salient feature of the hepatocytes is that they exhibit polyploidy(6). Immature
39 developing hepatocytes during the postnatal period (<21 days) are preferentially diploid, while the
40 mature hepatocytes are more polyploid(6, 7). In rodents, polyploidization starts around the time of
41 weaning, resulting in 80-90% of adult hepatocytes being polyploid(6). Some studies have
42 indicated a higher proliferation rate for diploid hepatocytes than polyploid hepatocytes(8, 9).
43 Contrastingly, other studies demonstrate that higher hepatocyte polyploidy supports the
44 adaptations during chronic liver injury or cancer by providing extra gene copies(6–8).
45 Nonetheless, polyploidy is conserved in the liver, but the mechanisms that link some of the
46 metabolic functions, such as detoxification, to polyploidy remain elusive.

47 A key xenosensor in the liver that transcriptionally regulates detox machinery is the
48 Constitutive Androstane Receptor (CAR or Nr1i3)(10). Upon activation, CAR translocates to the
49 nucleus, heterodimerizes with the Retinoid X receptor (RXR), and binds the xenobiotic response
50 element module (XREM) of the target genes(11–13). Besides detoxification, ligand-mediated
51 CAR activation is typically accompanied by hepatomegaly and increased DNA synthesis as
52 measured by Ki-67(14, 15). Moreover, synthetic CAR activators, TCPOBOP (TC), and
53 phenobarbital have been shown to increase hepatocyte ploidy(14). However, how these cells
54 respond to these CAR-mediated increases in DNA synthesis and increases in dNTP requirements
55 has not been fully examined.

56 We mined the publicly available transcriptome after CAR activation and found a robust
57 increase in *RRM2* (Ribonucleotide Reductase Regulatory subunit M2) transcripts. This gene
58 encodes the catalytic subunit of the rate-limiting enzyme ribonucleotide reductase, which converts
59 NDPs (Nucleoside diphosphates) to dNDPs (deoxynucleoside diphosphates) in the dNTP
60 synthesis pathway(16–18). Then, we investigated if CAR could bind and activate RRM2
61 transcription and scanned the 5' upstream region of the RRM2 gene. We performed luciferase and
62 chromatin immunoprecipitation assays, followed by PCR to validate the functionality of the
63 putative CAR binding site. We measured hepatic dNTP levels to corroborate our findings. We
64 then tested if ectopic expression of RRM2 in CAR knockouts (CARKO) alter proliferation or
65 ploidy status. Finally, we investigated if active RRM2 was necessary for facilitating CAR-
66 mediated DNA synthesis.

67 **Method**

68

69 **Mice experiment** – C57BL/6J mice were obtained from Jackson Laboratories, and CARKO mice
70 were obtained from Dr Moore's lab at Baylor College of Medicine. The age and sex of the mice
71 used for the experiments are mentioned in the figure legends. The mice were housed in a standard
72 12-hr light/dark cycle with chow food and water available ad libitum. All the mice used in the
73 study have complied with NIH guidelines for the care and use of laboratory animals, and
74 experiments were performed as directed by the Institutional Animal Care and Use Committee at
75 the University of Illinois, Urbana-Champaign. All mice were acclimatized to the facility at least 2
76 weeks prior to the experiments. Mouse CAR agonist, 1,4-bis[2-(3,5-dichloropyridyloxy)] benzene
77 (TCPOBOP, Sigma, #T1443), TC was dissolved in Cornoil and intraperitoneally (IP) injected at
78 100 mg/Kg once into the mice, euthanized after 3 days of treatment, and collected samples for
79 further studies. Mouse Rrm2 was overexpressed using AAV-DJ8 under the CAG promoter with
80 sfGFP at the C terminus (VB220927-1597gxb and VB220823-1142mex). Viruses were obtained
81 from the vector builder and were IP-injected at a concentration of 10^11 GC. The mice were
82 euthanized after two weeks for serum and liver collection.

83

84 **Cell culture –** AML12 cells were transfected with 1µg of pCMV-HA–mutRRM2 (mouse;
85 Y176F), pCMV-Myc–WT RRM2 (mouse), and pCMV-Flag–CAR (mouse) using Lipofectamine
86 3000 for 48 hr. For cotransfection, equal concentrations of individual plasmids were mixed to
87 achieve a total of 1 µg/well. Cells were serum-starved for 16 hr, reseeded at 40% confluence in
88 complete medium containing 10% serum with or without TC (250 nM) dissolved in DMSO, and
89 incubated for 16 hr before analysis. Aliquots of cells were collected at the time of reseeding for
90 immunoblot analysis.
91 Primary hepatocytes were isolated from WT mice using collagenase perfusion and were treated
92 with hydroxyurea (1mM) or TC - CAR ligand (250nM) or both for 6 hours, and cells were
93 harvested for RNA preparation and qPCR analysis.

94

95 **Molecular cloning** - Mouse and human CAR open reading frames (ORFs), including wild-type
96 (wtRRM2) and tyrosine-to-phenylalanine substitution mutants (mouse Y176F; human Y175F)
97 (mutRRM2), were synthesized (Twist Bioscience) and cloned into the BamHI–HindIII restriction
98 sites of the pcDNA3 expression vector(pCMV).

99 **Click-IT Plus Edu Staining –** Cell proliferation was assessed by incorporation of 5-ethynyl-2′-
100 deoxyuridine (EdU) during a 2-hr pulse(19). Cells were fixed with 4% paraformaldehyde, and
101 EdU detection was performed using click chemistry according to the manufacturer's instructions
102 (Thermo Fisher Scientific, # C10640).
103
104 **RNA extraction, cDNA synthesis, and qPCR** – RNA was isolated from the liver using TRIzol
105 (Invitrogen) according to the manufacturer's instructions. The quality of the RNA was measured
106 using the Bioanalyzer and 0.2% bleach gel. 3-5 µg of isolated RNA was used to synthesize the
107 cDNA with random primers (NEBiolabs) and the Maxima Reverse transcriptase kit (Thermo
108 Fisher Scientific). 50 ng of cDNA was used for every SYBR green kit (Thermo Fisher Scientific)
109 based qRT-PCR. Relative gene expression was calculated by the ΔCt or ΔΔCt method and
110 normalized to 36b4 or actin, as mentioned in the figure legends. qPCR primer details are listed in
111 the supplementary table.
112
113 **Luciferase assay** - HepG2 cells in a 6-well plate were transfected using calcium phosphate
114 precipitation as described in previous publications(20, 21). 0.1µg/well of luciferase reporter
115 (mRRM2- pTKLUC or mRRM2mutant-pTKLUC), 0.05µg/well of pCMX-CAR, 5ng/well of
116 RXR, and 0.1µg/well of β-gal were used for the luciferase assay. PGEM4 was used to scale the
117 total plasmid concentration to 5µg/well. 35 bp of the CAR response element identified in the
118 RRM2 promoter region was sequenced and cloned into TK-LUC for analysis. The mutant RRM2
119 CAR response element was generated by mutating the key GG nucleotides to AA. After
120 transfection, the cells were treated with TC: 250 nm overnight. Luciferase expression was assayed
121 and normalized using β-gal expression. All luciferase values were averaged from triplicate
122 samples. All transfection data were repeated at least three times.
123
124 **Western blot assay** – Protein lysates were made with RIPA buffer (25 mM Tris-HCl, 150 mM
125 NaCl, 0.5% Sodium deoxycholate, 1% Triton X-100, 0.1% SDS, 0.1 mL Phosphatase inhibitor,
126 and 1x protein inhibitor). A total of 25µg of liver tissue lysate or 30µg of cell lysate was loaded to
127 each lane and was separated with 10% SDS-PAGE. The proteins were then transferred to a
128 nitrocellulose membrane. After blocking with 5% non-fat milk in TBS, the membrane was probed
129 with a primary antibody overnight at 4 ^{0}C (Gapdh (# 2118, Cell Signaling, 1:5000 dilution),
130 RRM1 (# sc- 11733, Santa Cruz, 1:100 dilution), RRM2 (# sc- 10848, Santa Cruz, 1:100 dilution),

131 RRM2 (# sc- 398294, Santa Cruz, 1:100 dilution), Flag (# F1804, Sigma, 1:1000 dilution), HA (#
132 51064-2-AP, Proteintech, 1:5000 dilution), Myc (# sc-40, Santa Cruz, 1:1000 dilution), His (#
133 ab18184, Abcam, 1:1000 dilution) followed by secondary antibody 1 hr incubation at RT (anti-
134 mouse # 115-005-174, anti-rabbit # 111-005-045, anti-goat # 805-005-180 from Jackson
135 Immunoresearch at 1:5000 dilution). The membrane was developed with an enhanced
136 chemiluminescent detection reagent and imaged with X-ray film or a Bio-Rad ChemiDoc.
137
138 **Liver histology and staining** – Mouse liver tissues were fixed in 10% formalin at 4 ^{0}C for 12-24
139 hours, processed, and embedded in paraffin. 5 µm liver sections were made and deparaffinized in
140 xylene and hydrated in a series of graded alcohol and water. Standard hematoxylin and eosin
141 (H&E) staining was used to examine morphology. For immunohistochemistry (IHC), sections
142 were incubated with 3% hydrogen peroxide for 15 minutes to block endogenous peroxidase. In
143 both IHC and immunofluorescence (IF), the sections are heated in Tris-EDTA (pH 9.0) for 30
144 minutes for antigen retrieval, followed by 1 hour of blocking in 5% BSA and 2% NGS at 4 ^{0}C.
145 The sections were incubated with the primary antibody Ki-67 (# 550609, BD Bioscience, 1:100
146 dilution), PCNA (# sc- 25280, Santa Cruz, 1:750 dilution), pHH3 # PA5-17869, Invitrogen, 1:750
147 dilution), β-catenin (BDB610154, BD Bioscience, 1:1000 dilution), or H2A.X (ab11175, abcam,
148 1:500) at 4 ^{0}C overnight. After the TBS-0.025% Triton X-100 wash, samples were incubated with
149 horseradish peroxidase (HRP) anti-mouse (# 115-005-003, Jackson ImmunoResearch, 1:750
150 dilution) or anti-rabbit # 111-005-045, Jackson ImmunoResearch, 1:750 dilution) or anti-mouse
151 555 (# A-21424, Invitrogen, 1:1000 dilution) or anti-rabbit 555 (# A-21428, Invitrogen, 1:1000
152 dilution) fluorophore for 1 hour at RT. For IHC, the DAB staining kit (Vector Laboratories, #SK-
153 4100) was used according to the manufacturer's protocol. For IF, the sections were incubated with
154 NuBlue (Thermo Scientific, #R37605) for 30 minutes at room temperature, and the background
155 signals were quenched using Vector TrueVIEW Autofluorescence Quenching (#SP-8400-15) from
156 Vector Laboratories as per the instructions. The slides were viewed with Nanozoomer or the LSM
157 900 confocal microscope.
158
159 **Tunnel staining** – For checking the DNA damage, tunnel staining was performed with Click-iT™
160 Plus TUNEL Assay Kits (ThermoFisher Scientific, # C10617) as per the instructor's manual and
161 viewed under the LSM 900 microscope.
162

163 **Chromatin Immuno-Precipitation (ChIP)** – Briefly, the FLAG-CAR construct was transiently
164 transfected into HepG2 cells. After 24 hours of TC treatment, the FLAG-tagged CAR was pulled
165 down using an anti-FLAG antibody (Sigma, # F1840), followed by sonication and PCR
166 amplification of the RRM2 promoter region. 5'CTCCCAAAGTGCTGGGATTA3' and
167 5'CAAGCGACCAGGCTTCTTAC3' primers were used to for human RRM2 promoter DNA
168 fragments. All transfection and pull-down experiments were performed in three separate wells,
169 and IgG was used as a control.
170
171 **dNTP Pool analysis -** ~1g of liver tissue was washed with ice-cold 10mM Tris buffer, pH 7.3. 5x
172 volume of ice-cold Tris buffer relative to the weight of the tissue was added to the minced tissue,
173 and the mixture was homogenized completely. Cell debris was removed by centrifugation at 100g
174 for 10 minutes. Supernatant was transferred for further analysis and protein measurement. 100%
175 ice-cold methanol was added to the supernatant to obtain a final concentration of 60% methanol
176 (v/v), followed by incubation at 20 ^{0}C for 1 hr with intermediate vortexing. The samples were then
177 heated in boiling water for 3 minutes and centrifuged at 17,000 g for 15 minutes at 4 ^{0}C. The
178 resulting supernatant was transferred to a fresh tube and completely dried in a speed vacuum or
179 lyophilizer. The dried extracts were resuspended in water, and dNTP concentrations were
180 determined as previously described(22, 23).
181
182 **ChIP-seq data analysis** – We analyzed the BigWig and BED files (GSE112199) for YFP-tagged
183 mouse and human CAR ChIP-seq from Niu et al(24). Tracks were viewed on IGV aligned to
184 mm10 assembly.
185
186 **RNA-seq data analysis –** We analyzed the processed RNA sequencing file from WT mouse liver
187 treated with Cornoil or TC (GSE98666) by Cheng et al(25).
188
189 **Hepatocyte isolation** – Hepatocytes were isolated as described in Wilkinson et al(8).
190
191 **Ploidy analysis** – For detection of cellular ploidy, freshly isolated primary hepatocytes were stained
192 with 2 µl/ml Fixable Viability Dye (FVD) eFluor 780 (eBioscience, San Diego, CA) and 15 µg/ml
193 Hoechst 33342 (Life Technologies, Carlsbad, CA), as described(8). For nuclear ploidy, nuclei from
194 the frozen liver tissue were isolated as previously described(9, 26). - A piece of frozen liver tissue,

195 approximately 5 x 5 x 3 mm, was thawed at room temperature in 1 mL of PBS and chopped into
196 tiny pieces with a scalpel blade. The liver suspension was passed through a 20-gauge needle (10
197 times) and a 23-gauge needle (10 times) to break open cells. Suspensions were fixed overnight in
198 70% ethanol at 4°C, washed with PBS, centrifuged at 500g for 5 minutes at 4°C, and digested in
199 1.5mL pepsin (0.5mg/mL in 0.1N HCl, Millipore Sigma Life Science) for 20 minutes at RT to
200 generate nuclear suspensions. The nuclear suspensions were washed with 3 mL nuclear wash buffer
201 (PBS, 0.1% BSA, 0.5% Tween-20), incubated with 1.5 mL 2N HCl for 12 minutes at 37°C, washed
202 with 3mL cold borate buffer (6.25g H3BO3/L type I water, pH 8.5), and centrifuged at 500 g for 5
203 minutes at 4°C. The isolated nuclei were then stained with 5 µg/mL propidium iodide (Invitrogen,
204 Carlsbad, CA) in PBS with 250 µg/mL RNase A (Invitrogen) and analyzed with an LSR II flow
205 cytometer (BD Biosciences, Franklin Lakes, NJ) running BD FACSDiva™ Software pH v9.0.
206 FACS plots were generated using FlowJo 10.8.2 (FlowJo LLC, Ashland, OR)
207
208 **Image analysis software** –ImageJ was used to measure cellular area and quantify Ki-67, PCNA,
209 and pHH3 staining. QuPath is used to count the total cells.
210
211 **Statistical analyses.** All statistical analyses were performed using GraphPad PRISM (GraphPad
212 Software, Inc., La Jolla, CA). Data are presented as mean ± standard deviation (SD) or mean ±
213 standard error of the mean (SEM). Two-way ANOVA was performed unless mentioned in the figure
214 legends. Level of significance was $*P < 0.05$, $**P < 0.01$, $***P < 0.001$.

215 **Results and Discussion**

216

217 **Loss of CAR alters 2c and 4c ploidy status in the hepatocytes.**

218 As expected, CAR activation by TC results in an increased Ki-67 staining, hepatomegaly,
219 and robust induction of its downstream target genes, including *Cyp2b10,* Cyclin A (*CcnA*), and
220 Cyclin B (*CcnB*) in the liver(27, 28), and these responses are absent in the global CAR knockout
221 mice (CARKO) (Fig 1A, Supplementary Fig 1A- G). Besides these known targets, we found that
222 the E2F family of transcription factors (*E2f1* and *E2f8*), responsible for controlling liver
223 polyploidization, are upregulated in a CAR-dependent manner (Fig 1 B-C). Similarly, the
224 transcript levels of Aurora Kinase B (*AurkB*) and Polo-like kinase1 (*Plk1*), genes responsible for
225 the mitotic entry, are increased upon CAR activation(29) (Supplementary Fig 1 H-I). These
226 findings highlight a key role for CAR in regulating hepatic polyploidy. Next, we examined the
227 cellular ploidy of 5-week-old male WT and CARKO hepatocytes and found that deletion of CAR
228 resulted in higher 2c content that correlated with the reduction in 4c content. However, 8c and
229 16c proportions, which account for ~20-30% of the polyploid state, were not altered (Fig 1D-F).
230 Taken together, these findings suggest that CAR regulates transcriptional regulators of ploidy
231 and is necessary to maintain 2c and 4c-hepatocyte ratios (~70-80% of ploidy states) and their
232 distribution.

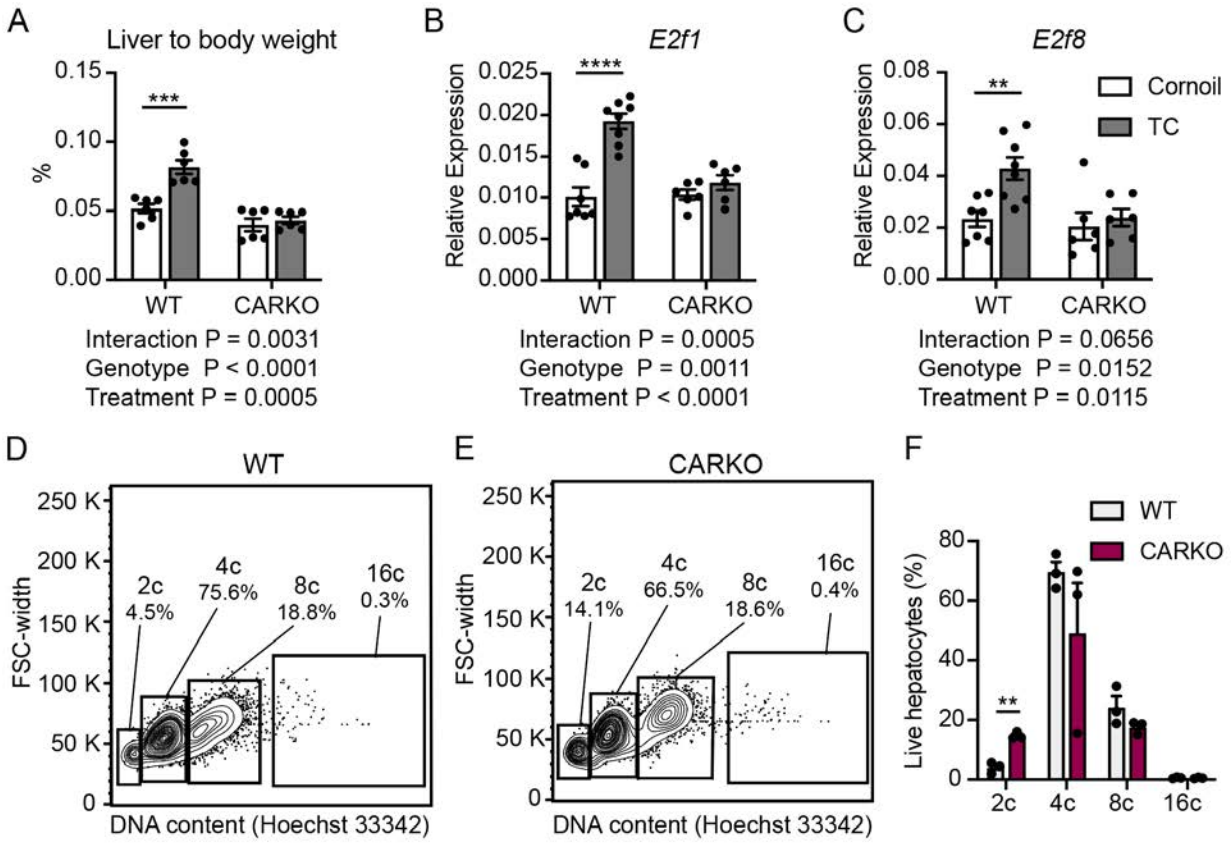

Figure 1 - Loss of CAR disrupts the mouse hepatocyte ploidy. (A) The liver-to-body weight ratio of WT and CARKO mice on CAR activation with TC or with control (Cornoil). (B-C) The transcript levels of ploidy-regulating genes *E12f1* and *E2f8* on CAR activation were analyzed using qPCR (n = 6-8 mice/group, adult male mice, 3-month-old; 36b4 was used as the internal control). Two-way ANOVA was performed for the statistical significance. (D and E) Isolated hepatocytes were isolated from 5-week-old male mice, FACS sorted, and used for cellular ploidy analysis. Representative images of gating channels for identifying the DNA content of WT (D) and CARKO (E) hepatocytes. (F) Quantification of live hepatocytes obtained from cellular ploidy analysis and unpaired two-tailed T-tests was used to perform the analysis, **p<0.005, ***p<0.0005.

246 **CAR regulates the transcription of the *Rrm2* gene.**

247 To investigate the mechanisms by which CAR activation promotes DNA synthesis and
248 subsequently ploidy, we mined publicly available CAR transcriptome accessible through the
249 Nuclear Receptor Signaling Website Atlas (NURSA)
250 (http://signalingpathways.org/datasets/dataset.jsf?doi=10.1621/datasets.01003), which looked at
251 post-3 days of TC treatment. Apart from the well-known increase in cyclin gene expression, we
252 noted an unexpected induction of ribonucleotide reductase subunits *Rrm1* and *Rrm2* in response
253 to TC treatment. The *Rrm1* gene encodes the substrate-binding domain, while the *Rrm2* gene
254 encodes the catalytic subunit of the rate-limiting enzyme in the *de novo* dNTP synthesis pathway
255 - Ribonucleotide reductase(17). We validated CAR-mediated induction of *Rrm1* and *Rrm2*
256 transcripts (Fig 2 A-B). Whereas the alternative subunit, *Rrm2b,* induced in response to DNA
257 damage(17, 30) was downregulated (Fig 2C). We also found that only the RRM2 protein was
258 increased upon CAR activation, not RRM1 (Fig 2D-F). These upregulations were absent in the
259 TC-treated CARKO mice, suggesting CAR was necessary for these transcript and protein
260 changes.

261 Based on these findings, we examined whether CAR directly regulates *Rrm2*
262 transcription. We screened the *Rrm2* promoter regions and identified putative CAR binding sites.
263 The putative CAR-binding DR3 motif (AGGT/GCA)(28) that was present 600 bp upstream in
264 the *Rrm2* promoter region was then cloned into the pTK-Luc vector (Fig 2G) to test its
265 functionality using a luciferase assay. CAR activation with TC led to a significant increase in
266 luciferase activity, which was lost when this DR3 site on *Rrm2* was mutated (Fig 2H),
267 confirming the transcriptional activation. We then tested if CAR directly binds to the *Rrm2*
268 promoter region using a chromatin immunoprecipitation PCR (ChIP-PCR). FLAG-tagged-CAR-
269 transfected HepG2 cells were treated with TC, and CAR was pulled down using the FLAG
270 antibody. ChIP-PCR analysis showed that ectopic expression of CAR was sufficient to allow its
271 binding to the *Rrm2* gene (Fig 2 I-J), irrespective of the presence or absence of TC. To further
272 validate these findings *in vivo*, we mined the previously published hepatic CAR ChIP-seq data
273 (Supplementary Fig 2), which was performed in CARKO supplemented with either mouse or
274 human CAR, followed by activation with their respective ligands(24). *Cyp2b10* was used as a
275 gold standard downstream CAR target, and as expected, it showed robust CAR binding peaks
276 upon activation with phenobarbital (PB), TC in mouse CAR, and CITCO in the humanized CAR

277 mice (Supplementary Fig 2A). Importantly, we found ligand-induced CAR binding peaks in
278 *Rrm2* were conserved in mice and human (Supplementary Fig 2C). These results demonstrate
279 that the CAR can bind and promote the transcription of the *Rrm2* gene.

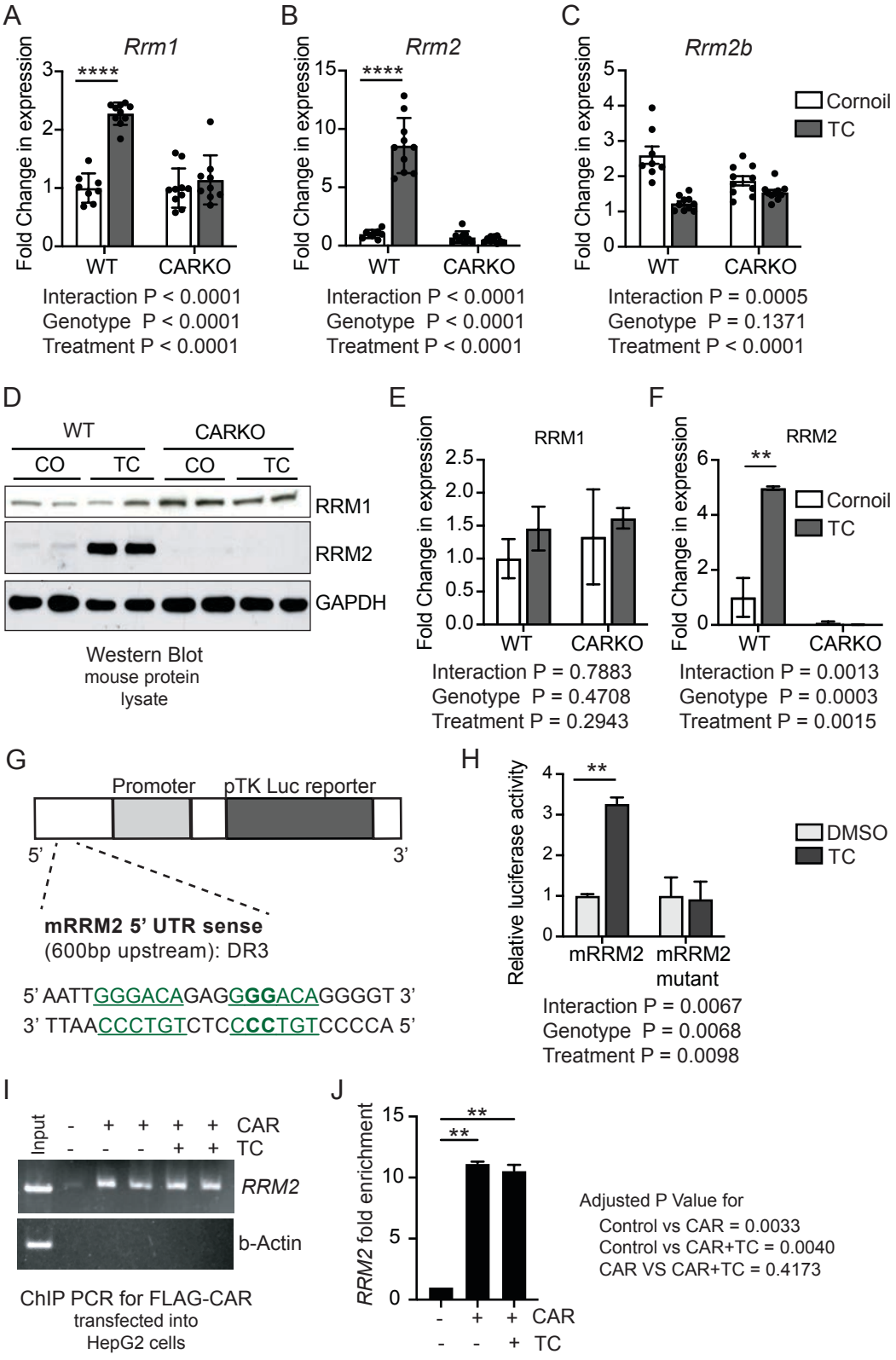
A
Rrm1
Fold Change in expression
****
WT
CARKO
Interaction P < 0.0001
Genotype P < 0.0001
Treatment P < 0.0001
B
Rrm2
Fold Change in expression
****
WT
CARKO
Interaction P < 0.0001
Genotype P < 0.0001
Treatment P < 0.0001
C
Rrm2b
Fold Change in expression
Cornoil
TC
WT
CARKO
Interaction P = 0.0005
Genotype P = 0.1371
Treatment P < 0.0001
D
WT
CARKO
CO
TC
CO
TC
RRM1
RRM2
GAPDH
Western Blot
mouse protein
lysate
E
RRM1
Fold Change in expression
WT
CARKO
Interaction P = 0.7883
Genotype P = 0.4708
Treatment P = 0.2943
F
RRM2
Fold Change in expression
**
Cornoil
TC
WT
CARKO
Interaction P = 0.0013
Genotype P = 0.0003
Treatment P = 0.0015
G
Promoter
pTK Luc reporter
5'
3'
mRRM2 5' UTR sense
(600bp upstream): DR3
5' AATTGGGACAGAGGGGACAGGGGT 3'
3' TTAACCCTGTCTCCCCTGTCCCCA 5'
H
Relative luciferase activity
**
DMSO
TC
mRRM2
mRRM2
mutant
Interaction P = 0.0067
Genotype P = 0.0068
Treatment P = 0.0098
I
Input
CAR
TC
RRM2
b-Actin
ChIP PCR for FLAG-CAR
transfected into
HepG2 cells
J
RRM2 fold enrichment
**
**
CAR
TC
Adjusted P Value for
Control vs CAR = 0.0033
Control vs CAR+TC = 0.0040
CAR VS CAR+TC = 0.4173

282 **Figure 2 - CAR binds and transactivates *RRM2* expression.** Transcript expression levels of
283 the ribonucleotide reductase subunit, *Rrm1* (A), and *Rrm2* (B) were analyzed using qPCR. (C)
284 *Rrm2b*, an alternative subunit of ribonucleotide reductase, was also measured by qPCR. (n = 8-
285 10 mice/group, 3-month-old male mice; β-actin was used as the internal control for qPCR
286 analysis) Two-way ANOVA was performed, and graphs are represented as mean ± SEM. (D)
287 Immunoblot analysis of RRM1 and RRM2 in the mouse liver lysates with and without TC
288 treatment and (E-F) normalized quantification are represented as mean ± SD. (G) Schematic
289 representation of the luciferase assay and the target RRM2 site sequence used for the assay. The
290 mutated sites for mRRM2 mutants are marked in **bold** and (H) the quantification represented as
291 mean ± SEM. (I-J) FLAG-tagged CAR construct was transfected into HepG2 cells, and the
292 expressed FLAG-CAR proteins were pulled down to perform ChIP. ChIP-PCR was performed
293 for the analysis (I) and quantified (J), and the graph is represented as mean ± SD (n = 3 technical
294 replicates). Two-way ANOVA was performed on A-C, E-F, and H, while One-way ANOVA
295 was performed on J.
296
297
298 **Activation of CAR upregulates the *de novo* dNTP synthesis pathway.**
299 We next tested if CAR activation regulated other genes encoding enzymes in the dNTP
300 metabolic pathway besides the rate-limiting catalytic subunit of ribonucleotide reductase, *Rrm2*.
301 To test this, we mined previously published bulk RNA sequencing data after TC treatment(25).
302 Our analysis revealed that apart from the expected increases in cyclins, CAR regulated the entire
303 dNTP pathway from synthesis to salvage, as well as genes involved in ploidy and cytokinesis
304 (Supplementary Fig 3). We first focused on dNTP synthesis and validated many of these changes
305 with qPCR.
306 dNTP synthesis pathway includes several steps, with ATIC (5-aminoimidazole-4-
307 carboxamide ribonucleotide formyltransferase/IMP cyclohydrolase) and UMP synthase (Uridine
308 monophosphate) being responsible for *de novo* purine and pyrimidine biosynthesis pathways,
309 respectively(31, 32). Briefly, IMPs are converted to ADPs (Adenose diphosphate) or GDPs
310 (Guanosine diphosphate), while UMPs are converted to UDP (Uridine diphosphate) and to UTP
311 (Uridine triphosphate), which is then acted upon by CTP synthetase to generate CTP (Cytidine
312 triphosphate). Ribonucleotide reductase subsequently reduces these substrates to their respective

313 dNDPs (deoxynucleoside diphosphate)(33). dCMP deaminase enzyme keeps the pyrimidine
314 dNTP pool by converting dCMP to dUMP, which in turn can be further modified to dTDP by
315 deoxythymidylate (dTMP) kinase and finally to dNTPs via NDP (nucleoside diphosphate) kinase
316 (Figure 3 A).
317 TC treatment in WT mice resulted in the upregulation of transcripts encoding for these
318 key enzymes – ATIC, UMP synthase, CTP synthetase, NDP kinase, dCMP deaminase, and
319 dTMP kinase in the liver (Figure 3 B-G). Despite the CAR-independent increase in NDP kinase,
320 induction of other enzymes was lost in the CARKO, indicating CAR dependency and
321 highlighting that CAR may regulate the expression of genes in the entire dNTP synthesis
322 pathway. Moreover, ChIP-seq data revealed that several genes (*Rrm2, Atic, NDP kinase encoded*
323 *by Nme1*) involved in dNTP synthesis exhibited CAR binding peaks (Supplementary Fig 2 C-E),
324 validating our data(24).
325 Based on these results, we examined the dNTP pools in the liver tissue with and without
326 CAR activation. Consistent with the transcriptional data, dATP and dTTP levels were robustly
327 induced in a CAR-dependent manner (Figure 3 H and J). Intriguingly, the dCTP and dGTP levels
328 were unchanged. One possibility is that the dGTP are present in high concentrations (~1 pg/mg
329 of protein) in the liver subsequent to enriched mitochondria pool(34) (Figure 3I). Whereas dCTP
330 levels may be converted to dTTP due to increase dCMP deaminase transcript (Figure 3 K).
331 Another possibility is the dATP is a known allosteric inhibitor of RRM2 activity(35, 36), thus an
332 increase in dATP will in turn inhibit RRM2 levels. Nonetheless, these results uncover that CAR
333 activation upregulates dNTP synthesis genes and certain dNTP pools.
334

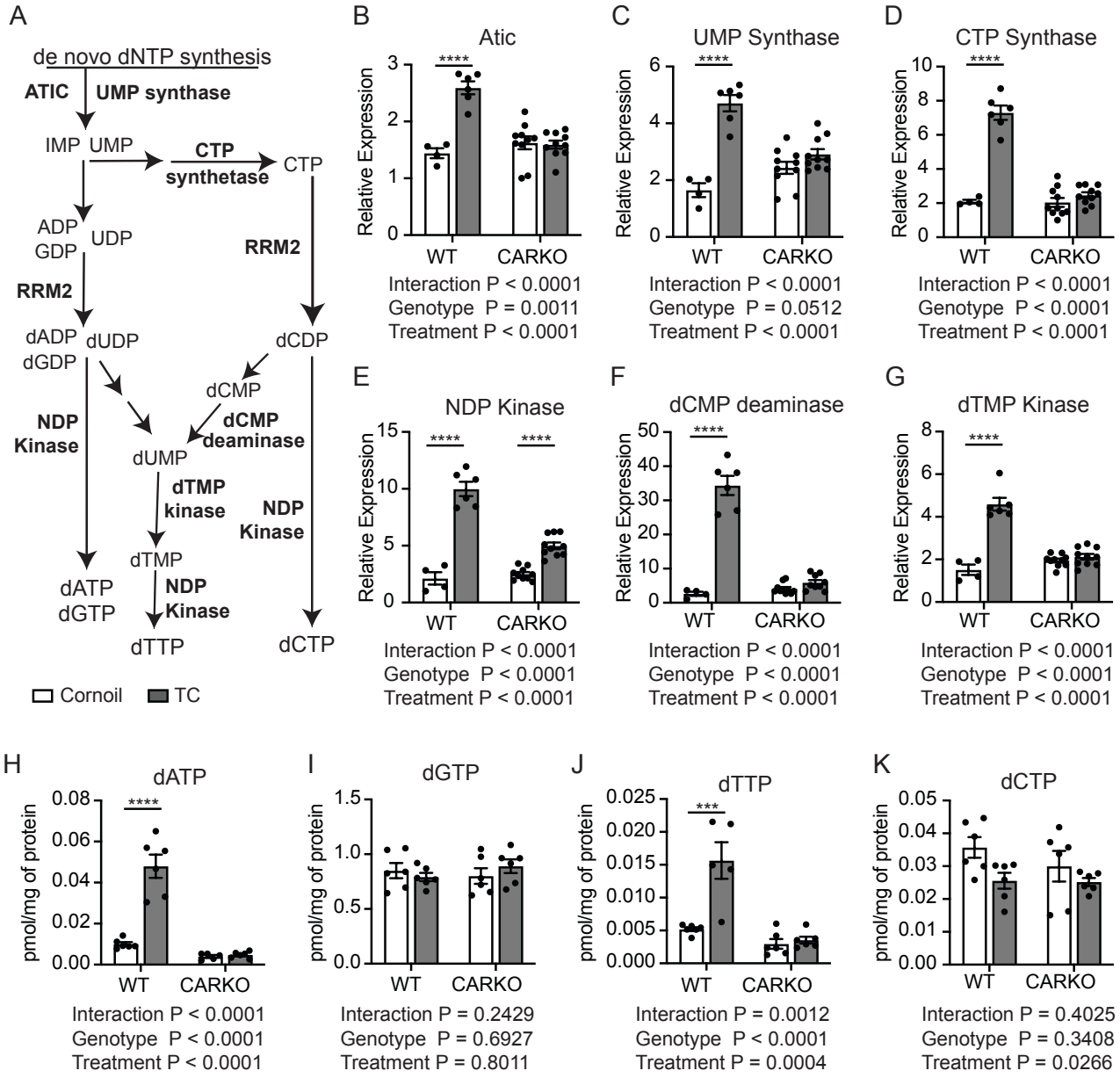

Figure 3. CAR activation increases key enzyme transcript levels in the *de novo* dNTP synthesis pathways. (A) Schematic representation of the crucial enzymes involved in the de novo dNTP synthesis pathway. (B-G) Transcript levels of these enzymes – ATIC (B), UMP Synthase (C), CTP Synthase (D), NDP Kinase (E), dCMP deaminase (F), dTMP Kinase (G) were measured using qPCR post-3 days of TC treatment. (n = 4-6, 3-month-old male mice, b-actin was used as the internal control for qPCR analysis). (H-K) Nucleotide (dATP (H), dGTP (I), dTTP (J), dCTP (K)) levels were analyzed from the liver tissue on CAR activation (n = 4-6

344 mice/group, 3-month male mice, normalized to the total protein of the liver sample). Two-
345 ANOVA was performed and all the graphs are represented as mean ± SEM.
346
347
348 **Ectopic RRM2 expression induces DNA synthesis and alters ploidy in CARKO**
349 **hepatocytes.**
350 Since RRM2 mediates the rate-limiting step for *de novo* dNTP synthesis(37), we
351 examined whether overexpressing (OE) RRM2 in the CARKO mice can compensate for ploidy
352 loss and promote DNA synthesis. Using AAV machinery, we introduced a 10^11 GC virus
353 carrying RRM2-GFP or Control-GFP construct into the mice and ensured that this did not cause
354 overt inflammation (Supplementary Fig 4 A-D). As expected, compared to the control-GFP
355 virus, RRM2-AAV led to a robust increase in *Rrm2* mRNA in WT and CARKO mice, ~10 fold
356 and 6-fold respectively (Fig 4 A). Importantly, RRM2 overexpression did not change the *Rrm2b*
357 or *Rrm1* transcript levels in both WT and CARKO mice, indicative of specificity of this
358 overexpression with no compensatory impact on other subunits (Fig 4 B, Supplementary Fig 4
359 E). We validated the RRM2-GFP expression in the livers of WT and CARKO mice by imaging
360 isolated primary hepatocytes. Despite a lower fold increase in *Rrm2* transcript levels in CARKO,
361 we observed no significant change in the RRM2-GFP expression compared to WT. (Fig 4 D)
362 Nonetheless, we were surprised to notice an 18% increase in the liver-to-body weight
363 ratio in CARKOs but not in the WT mice (Fig 4 C, Supplementary Fig 4 F-G). To examine if
364 there was excessive DNA synthesis upon RRM2 OE in CARKO, we used the DNA synthesis
365 marker, Ki-67 and PCNA which stains the entire cell cycle but with high intensity in the S
366 phase(38–40). RRM2 OE dramatically increased the percentage of Ki-67 and PCNA positive
367 nuclei, specifically in CARKO (~2 fold) compared to WT mice (Fig 4 E-H, Supplementary Fig 5
368 A-D, Supplementary Fig 6). Intriguingly, despite higher staining of these markers, the total
369 number of cells in the given microscopic field in CARKO was lower (Fig 4 I). Furthermore,
370 when we measured the hepatocyte cellular area on RRM2 OE using β-catenin staining, CARKO
371 exhibited larger hepatocytes compared to WT (Fig 4 J, Supplementary Fig 5 E-H). Overall, these
372 experiments show that introducing RRM2 in CARKO is sufficient to increase DNA synthesis,
373 cellular area, and, subsequently, the hepatosomatic index (liver-to-body weight ratio).

374 In WT adult mouse livers, approximately 80-90% of hepatocytes are polyploid. Further,
375 hepatocytes can be mono- or binucleate, resulting in varying cellular and nuclear ploidy(7, 41).
376 For instance, a tetraploid can be 4c in a mononucleate or 2c in a binucleate cell; an octoploid can
377 be 8c in a mononucleate or 4c in a binucleate cell, and so on. Hence, the percentage of 2c in
378 nuclear ploidy analysis will be higher than the cellular ploidy. As expected, nuclear ploidy
379 distribution differs from the cellular ploidy shown earlier. In nuclear ploidy, 2c and 4c nuclear
380 content comprises ≥90 percent of all the nuclei. Nuclear ploidy was assessed in frozen liver
381 samples that were also used for transcriptional analysis elsewhere. RRM2 OE in WT mice did
382 not alter nuclear ploidy status in the hepatocytes (Supplementary Fig 7 A, C). However, in the
383 CARKO hepatocytes, RRM2 OE restored the nuclear 2c and 4c to WT levels (Supplementary
384 Fig 7 B-C). This data is consistent, as most tetraploid hepatocytes (70-80%) are binucleate with
385 diploid nuclei, which explains the increase in 2c nuclei in the CARKO RRM2 OE group.
386 Likewise, as most octoploid hepatocytes are binucleate with tetraploid nuclei, this may lead to a
387 decrease in 4c nuclei.
388 Additionally, in a separate cohort of mice, we also determined cellular ploidy after
389 RRM2 OE. Although RRM2 OE increased the number of 2c hepatocytes in both genotypes, this
390 increase was insignificant (Fig 4 K-N). However, ectopic expression of RRM2 in CARKO
391 increased the percentage of 4c and 8c hepatocytes. Both these changes in the CARKO were
392 comparable to those of WT mice treated with RRM2. Nonetheless, RRM2 OE in CARKO results
393 in higher Ki-67 staining, increased 2c nuclei, and increased 2c hepatocytes.
394 Unlike 5-week-old mice, whose livers are still maturing, 16-week-old adult livers are in a
395 quiescent state and exhibit a different ploidy distribution. We found that the older adult mice
396 displayed more 8c hepatocytes, which is consistent with a concomitant decrease in 4c
397 hepatocytes (Supplementary Fig 6 D). In the CARKOs, we noticed that 2c hepatocytes
398 significantly dropped with aging from 14.1% to 4.3% (Fig 1 E-F and Fig 4 L, N), indicating that
399 ploidy "catches up" over time.
400 Since ploidy can be altered with pathological conditions(7, 41), we examined whether
401 this change in the ploidy seen in WT and CARKO post-RRM2 OE was pathological by tunnel
402 and H2Ax staining for DNA damage. We found no immunostaining differences between the
403 control and RRM2 OE, negating the role of pathological ploidy changes; rather, they are driven

404 by RRM2 OE (Supplementary Fig 7 E-F). Collectively, these data suggest that the CAR
405 contributes towards dNTP synthesis and hepatocyte ploidy via RRM2.
406

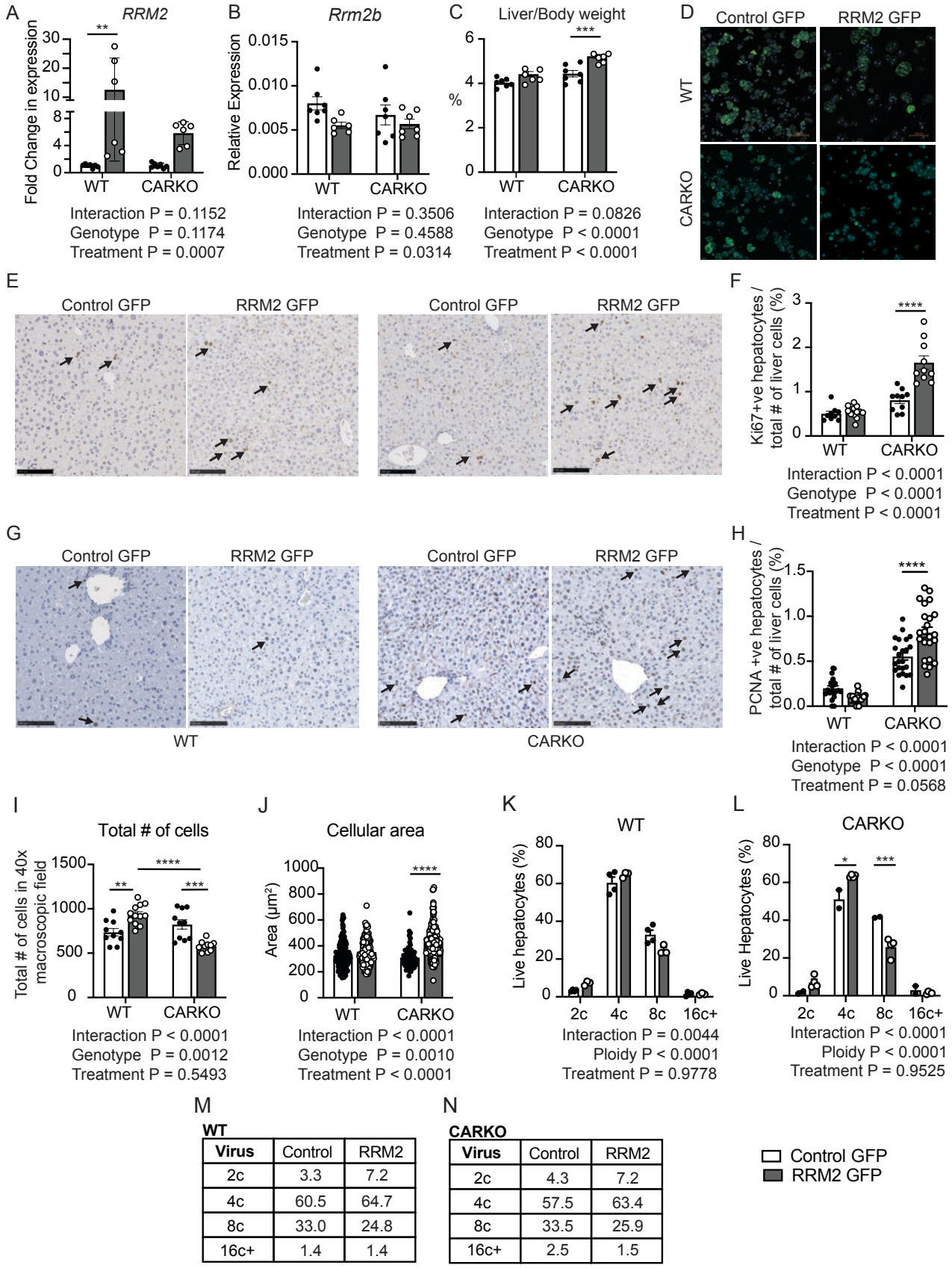

M

WT

Virus	Control	RRM2
2c	3.3	7.2
4c	60.5	64.7
8c	33.0	24.8
16c+	1.4	1.4

N

CARKO

Virus	Control	RRM2
2c	4.3	7.2
4c	57.5	63.4
8c	33.5	25.9
16c+	2.5	1.5

408 **Fig 4 – Overexpression of RRM2 in CARKO increases hepatocyte proliferation and alters**
409 **cellular ploidy.** Transcript levels of *Rrm2* (A) and *Rrm2b* (B) from WT and CARKO mice livers
410 treated with Control GFP or RRM2-GFP. (n = 6-8 mice/group, 4-month-old female mice, 36b4
411 was used as the internal control for qPCR analysis). (C) The liver-to-body weight ratio for the
412 virus-treated mice. (D) Hepatocytes from mice treated with control-GFP and RRM2-GFP virus
413 were isolated with a 2-step collagenase perfusion. These cells were incubated with DAPI (blue)
414 and viewed under a microscope for GFP or RRM2-GFP (green) expression. Representative
415 images of (E) Ki-67 and (G) PCNA from WT and CARKO liver treated with control GFP or
416 RRM2-GFP. Black arrows point to the Ki-67 or PCNA staining. Quantification of (F) Ki-67 and
417 (H) PCNA -positive hepatocytes in the liver section was normalized to the total number of cells
418 under the focus region. (I) Total number of cells under the 40x Microscopic field in the liver
419 sections. (J) Liver sections were stained with β-catenin and DAPI, and each cell's cellular area
420 was measured with ImageJ software. (n = 6-8 mice/group, technical replicate = 3 per group). (K-
421 L) Cellular ploidy quantification for WT and CARKO with control GFP or RRM2-GFP.
422 Hepatocytes were isolated by 2-step collagenase perfusion and proceeded for FACS sorting and
423 ploidy analysis. (M-N) Average of cellular ploidy of WT (M) and CARKO (N) across 2-3
424 samples per group. Two-way ANOVA was performed for all the analyses, and the graphs are
425 expressed as mean±SEM.

426 **Active RRM2 is necessary for CAR-mediated DNA synthesis**

427 Finally, we tested the dependence of CAR on RRM2 function in orchestrating cellular
428 proliferation. We transiently inhibited RRM2 using hydroxyurea (HU) and tested for TC-
429 mediated CAR activation in primary mouse hepatocytes. As expected, TC induced
430 *Rrm2, Ccnb1,* and dNTP synthesis gene transcripts in cultured WT hepatocytes. Importantly,
431 these upregulations were lost upon co-treatment with HU (Figure 5A), underscoring the
432 relevance of RRM2 in facilitating CAR responses. But this still did not directly assess for DNA
433 synthesis upon CAR activation. Therefore, we performed an EdU incorporation experiment with
434 and without functional RRM2 by generating wtRRM2 and catalytically inactive RRM2(42, 43)
435 (mouse Y176F) constructs (Fig 5 B-D, Supplementary Fig 9). Since the transfection efficiency of
436 multiple plasmids are technically challenging in primary hepatocytes, we utilized AML12, an
437 immortalized non-tumorigenic mouse hepatocyte cell line, for our studies. We also took
438 advantage of the fact that these cells had poor expression of RRM2, consistent with the quiescent
439 hepatocytes under normal physiology. Transfecting these cells with CAR did not alter EdU
440 incorporation, whereas introducing wtRRM2 increased it, which was further amplified by co-
441 transfecting CAR and wtRRM2 (Fig 5 B-C, Supplementary Fig 9 A-B). This increase was
442 completely lost when mutRRM2 (Y176F) was co-transfected with CAR, but the reintroduction
443 of wtRRM2 restored it (Fig 5 B-C, Supplementary Fig 9 A-B). Next, we examined DNA
444 synthesis upon CAR activation under this same experimental paradigm. Activating CAR
445 increased EdU incorporation as expected, and it was dampened in the presence of mutRRM2.
446 Although wtRRM2 supplementation to mutRRM2+CAR revealed higher EdU incorporation,
447 unlike the basal conditions, it did not fully compensate for it (Fig 5 B-D, Supplementary Fig 9 A-
448 C). Taken together, these data provide compelling evidence that catalytically inactive RRM2 can
449 dampen CAR-mediated DNA synthesis.

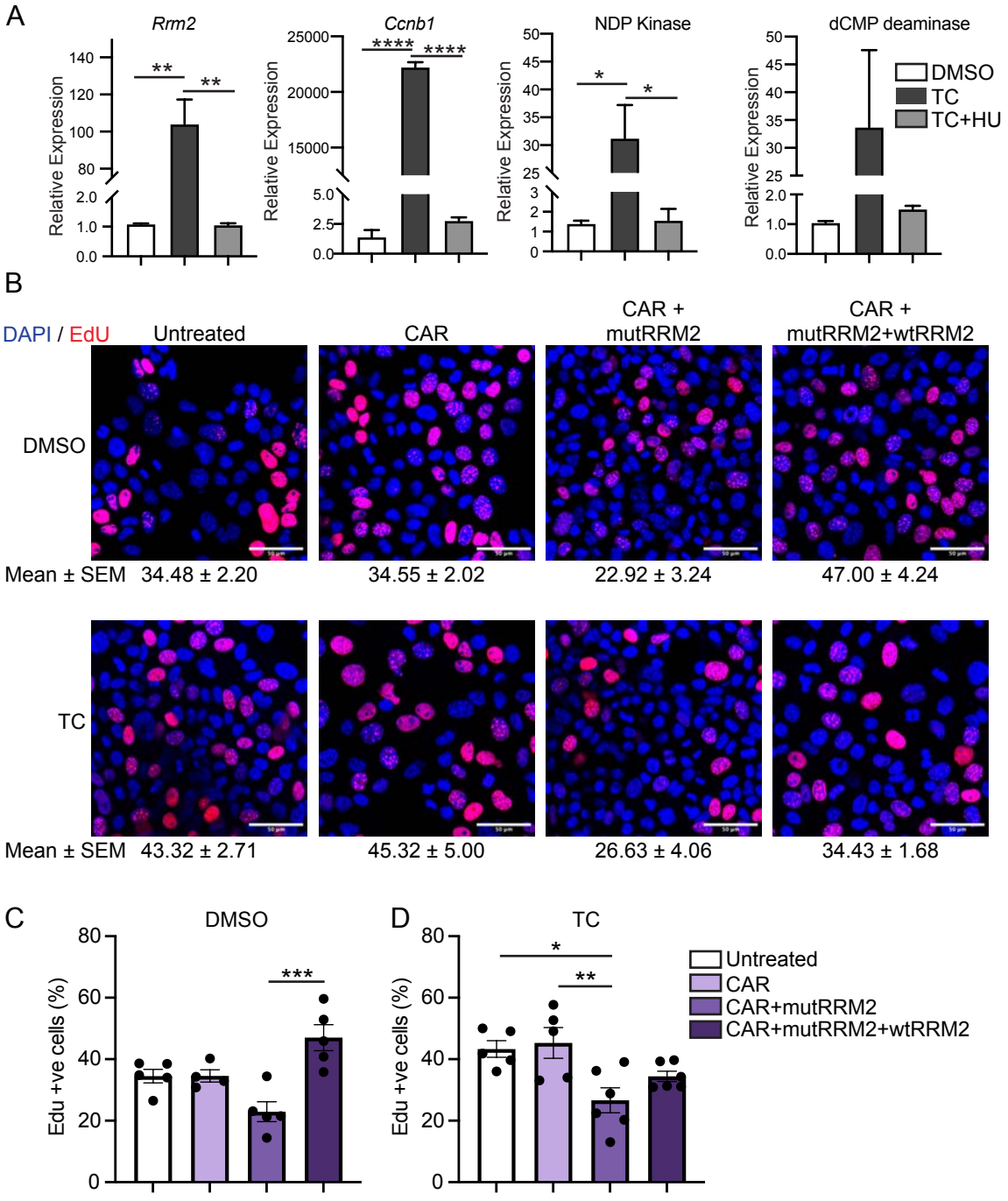

Fig 5 –CAR-mediated DNA synthesis is dependent on catalytically active RRM2. (A) Hepatocytes isolated from WT mice were treated with HU or TC, and the transcript levels of *Rrm2*, *Ccnb1*, NDP Kinase, and dCMP deaminase were measured by qPCR, with β-actin as the internal control (n=3 mice/group). One-way ANOVA was performed, and the graphs show mean ± SEM. (B) Representative images of Edu incorporated (Edu in red and DAPI in blue) into the

457 AML12 cells transfected with the CAR, WT RRM2 (wtRRM2), and Y176F mutant RRM2
458 (mutRRM2) constructs. The top panel corresponds to the DMSO, while the bottom panel
459 corresponds to the TC treatments. (C-D) Quantification of Edu positive cells to the total number
460 of cells under DMSO (C) and TC (D) treatment. One-way ANOVA was performed, and graphs
461 are presented as mean±SEM.
462
463 **Discussion**
464 In rodents, transient CAR activation results in hepatomegaly, increased Ki-67 staining,
465 and is linked to higher polyploidy, while prolonged activation results in liver cancer(14, 44).
466 Although *FoxM1, Mdm2,* and *cMyc* signaling are implicated in facilitating CAR-driven liver
467 proliferation, how CAR orchestrates DNA synthesis and ploidy remains unknown. Here, we
468 identified a new CAR target, *Rrm2*, which encodes the catalytic subunit of the ribonucleotide
469 reductase complex that is essential for *de novo* dNTP synthesis. Additionally, ligand activation
470 of CAR was sufficient to induce several genes involved in dNTP biosynthesis. All these effects
471 were absent in CARKO mice. We have not investigated if all these dNTP biosynthesis genes are
472 direct or indirect targets of CAR. But one of the key rate-limiting steps is catalyzed by
473 ribonucleotide reductase, and we demonstrate that CAR directly regulates the RRM2 subunit.
474 With respect to ploidy, CAR has been thought to increase ploidy by facilitating the
475 endoreduplication of DNA(14). Here, we show that CAR can regulate various aspects of hepatic
476 polyploidization. We found that CAR activation induces the *E2f* family of transcription factors,
477 for instance, *E2f1* promotes polyploidization while *E2f*8 inhibits it. Moreover, we find that
478 cytokinesis mediators- *Aurkb* and *Plk1* transcripts are also induced in a CAR-dependent manner.
479 Thus, CAR may transcriptionally control several aspects of liver polyploidization and may
480 contribute to maintaining overall ploidy distribution.
481 We validated that dNTP levels in livers were higher post-CAR activation, which is
482 consistent with the *Rrm2* gene and protein induction. We find a significant increase in dATP and
483 dTTP levels. dATP, in turn, can act as an allosteric inhibitor of RRM2 activity(36). Thus, RRM2
484 expression and activity are tightly controlled. One possibility is that the RRM2 increase seen in
485 TC treatment is secondary to cell cycle activation to promote DNA synthesis. So, we tested the
486 consequence of OE of RRM2 in quiescent CARKO livers from adult mice. We note that control
487 viral treatments, as expected, result in a mild pro-proliferative response in both genotypes. While

488 RRM2 OE in WT mice led to Ki-67 staining comparable to that of GFP virus-treated mice, in
489 CARKO, it robustly amplified Ki-67 staining, indicating increased DNA synthesis in CARKO.
490 PCNA also showed a similar pattern to Ki-67, except for higher basal staining with GFP virus-in
491 CARKO. This could be due to PCNA staining not being restricted to the S phase. Therefore, the
492 increased PCNA and Ki-67 staining in CARKO suggests that RRM2OE is sufficient to increase
493 DNA synthesis, change ploidy, and affect the overall liver status size. Since other RRM subunits,
494 especially *Rrm2b*, exhibit compensatory effects, we measured *Rrm1* and *Rrm2b* and found their
495 levels unchanged upon RRM2 OE (Fig 4B, Supplementary Fig 4E).
496 A limitation of this study is that we do not fully understand how RRM2 OE promotes this
497 heightened expression of S-phase markers in CARKOs. First, we examined the transcripts
498 involved in the dNTP synthesis pathway. Post RRM2 OE, there was no change except for a
499 reduction in UMP synthetase and dTMP kinase transcripts, indicative of a potential
500 compensatory effect (Supplementary Fig 8 A-F). Similarly, cell cycle pathway genes were
501 examined, and we found that S-phase cyclins (*Ccna1* and *Ccne1*) were increased in CARKO
502 (Supplementary Fig. 8 G-H), which is consistent with the higher Ki-67 staining. However, the
503 *E2f1* and *E2f8* transcripts did not change post-RRM2 OE in WT and CARKO livers
504 (Supplementary Fig 8 I-J). These findings indicate that the ectopic introduction of RRM2 is
505 sufficient to alter genes involved in the *de novo* dNTP biosynthesis pathway and S-phase cyclins,
506 mainly in CARKO.
507 In terms of ploidy, RRM2 OE in the absence of CAR increased diploid nuclear content
508 that coincided with the decrease in tetraploid nuclear content (Supplementary Fig 7 B-C). The
509 cellular ploidy of CARKO RRM2 OE mimicked that of WT RRM2 OE, suggesting the CAR-
510 mediated RRM2 expression is essential in maintaining the liver ploidy status (Fig 4 K-N).
511 Polyploid hepatocytes have been shown to have a distinct metabolic capacity(7, 8, 45) and are in
512 line with the xenosensing function of CAR.
513 We demonstrate that CAR promotes DNA synthesis directly, as measured by EdU
514 incorporation, and that this increase is contingent on the presence of a functional RRM2, as
515 transfection of a catalytically inactive RRM2 quenched EdU labeling observed upon co-
516 transfection of CAR and wtRRM2. Overall, these data clearly show that CAR-RRM2 signaling
517 may coordinate liver proliferation and polyploidy status and that CAR may play a basal role in
518 maintaining liver ploidy status during development.

519 **Data Availability**

520 All data produced in this study are included in the article and in its online supplementary
521 material.

522

523 **Acknowledgements**

524 We would like to thank Dr Chang Cui, Department of Biochemistry, UIUC, for helping in
525 critically interpreting RRM2 overexpression data and for sharing RRM2 constructs and
526 suggesting appropriate catalytically inactive RRM2 mutants. We also thank
527 Dr. Auinash Kalsotra, Department of Biochemistry, UIUC, for valuable advice, resources and
528 inputs throughout this project. Core Facilities at the Carl R. Woese Institute for Genomic
529 Biology, at the UIUC and at The University of Pittsburgh Unified Flow Core
530 (RRID:SCR_025102) supported this project.

531

532 **Authors Contribution**

533 S.A conceived, conceptualized and obtained funding for this study. A.A., B.M., and S.A.
534 planned and designed the experiments for this study. D.D.M was involved in
535 the initial study design. S.A performed the initial protein, RNA, ChIP and luciferase
536 analysis. B.M. and A.C. performed the *de novo* dNTP pathway analysis. L.W. and C.K.M.
537 performed the dNTP analysis. F.A. and A.W.D. performed all the FACS sorting and ploidy data
538 analysis. B.M., A.A. and B.C. isolated hepatocytes and nuclei for FACS analysis. A.A. and S.A.
539 designed and carried out the experiments for overexpression studies. B.M, and A.C performed
540 RRM2 inhibitor studies. S.C. did all the transfections for EdU staining and S.C and A.A imaged
541 and analyzed the data. A.A., A.W.D and S.A. wrote the manuscript with suggested edits by all
542 the authors.

543

544 **Funding**

545 This work was supported by NIH grants R01DK113080 (to SA), R01DK103645 (to AWD) and
546 the Pittsburgh Liver Research Center Clinical Biospecimen and Processing Core
547 (P30DK120531).

548

549 **References**

550 1. Forbes,S.J. and Newsome,P.N. (2016) Liver regeneration — mechanisms and models to
551 clinical application. *Nat Rev Gastroenterol Hepatol*, **13**, 473–485.

552 2. Michalopoulos,G.K. and Bhushan,B. (2021) Liver regeneration: biological and pathological
553 mechanisms and implications. *Nature Reviews Gastroenterology & Hepatology*, **18**, 40–55.

554 3. Bogdanos,D.P., Gao,B. and Gershwin,M.E. (2013) Liver Immunology. *Compr Physiol*, **3**,
555 567–598.

556 4. Blouin,A., Bolender,R.P. and Weibel,E.R. (1977) Distribution of organelles and membranes
557 between hepatocytes and nonhepatocytes in the rat liver parenchyma. A stereological study. *J*
558 *Cell Biol*, **72**, 441–455.

559 5. Mendoza,R., Banerjee,I., Reghupaty,S.C., Yetirajam,R., Manna,D. and Sarkar,D. (2022)
560 Isolation and Culture of Mouse Hepatocytes and Kupffer Cells (KCs). *Methods Mol Biol*,
561 **2455**, 73–84.

562 6. Donne,R., Saroul-Aïnama,M., Cordier,P., Celton-Morizur,S. and Desdouets,C. (2020)
563 Polyploidy in liver development, homeostasis and disease. *Nat Rev Gastroenterol Hepatol*, **17**,
564 391–405.

565 7. Wang,M.-J., Chen,F., Lau,J.T.Y. and Hu,Y.-P. (2017) Hepatocyte polyploidization and its
566 association with pathophysiological processes. *Cell Death Dis*, **8**, e2805–e2805.

567 8. Wilkinson,P.D., Delgado,E.R., Alencastro,F., Leek,M.P., Roy,N., Weirich,M.P., Stahl,E.C.,
568 Otero,P.A., Chen,M.I., Brown,W.K., *et al.* (2019) The Polyploid State Restricts Hepatocyte
569 Proliferation and Liver Regeneration in Mice. *Hepatology*, **69**, 1242–1258.

570 9. Pandit,S.K., Westendorp,B., Nantasanti,S., van Liere,E., Tooten,P.C.J., Cornelissen,P.W.A.,
571 Toussaint,M.J.M., Lamers,W.H. and de Bruin,A. (2012) E2F8 is essential for polyploidization
572 in mammalian cells. *Nat Cell Biol*, **14**, 1181–1191.

573 10. Wei,P., Zhang,J., Egan-Hafley,M., Liang,S. and Moore,D.D. (2000) The nuclear receptor
574 CAR mediates specific xenobiotic induction of drug metabolism. *Nature*, **407**, 920–923.

575 11. Kawamoto,T., Sueyoshi,T., Zelko,I., Moore,R., Washburn,K. and Negishi,M. (1999)
576 Phenobarbital-Responsive Nuclear Translocation of the Receptor CAR in Induction of the
577 CYP2B Gene. *Molecular and Cellular Biology*, **19**, 6318–6322.

578 12. Yoshinari,K., Kobayashi,K., Moore,R., Kawamoto,T. and Negishi,M. (2003) Identification of
579 the nuclear receptor CAR:HSP90 complex in mouse liver and recruitment of protein
580 phosphatase 2A in response to phenobarbital. *FEBS Letters*, **548**, 17–20.

581 13. Kobayashi,K., Sueyoshi,T., Inoue,K., Moore,R. and Negishi,M. (2003) Cytoplasmic
582 Accumulation of the Nuclear Receptor CAR by a Tetratricopeptide Repeat Protein in HepG2
583 Cells. *Mol Pharmacol*, **64**, 1069–1075.

584 14. Huang,W., Zhang,J., Washington,M., Liu,J., Parant,J.M., Lozano,G. and Moore,D.D. (2005)
585 Xenobiotic Stress Induces Hepatomegaly and Liver Tumors via the Nuclear Receptor
586 Constitutive Androstane Receptor. *Molecular Endocrinology*, **19**, 1646–1653.

587 15. Shizu,R., Benoki,S., Numakura,Y., Kodama,S., Miyata,M., Yamazoe,Y. and Yoshinari,K.
588 (2013) Xenobiotic-Induced Hepatocyte Proliferation Associated with Constitutive
589 Active/Androstane Receptor (CAR) or Peroxisome Proliferator-Activated Receptor α
590 (PPARα) Is Enhanced by Pregnane X Receptor (PXR) Activation in Mice. *PLOS ONE*, **8**,
591 e61802.

592 16. Nordlund,P. and Reichard,P. (2006) Ribonucleotide Reductases. *Annual Review of*
593 *Biochemistry*, **75**, 681–706.

594 17. Aye,Y., Li,M., Long,M.J.C. and Weiss,R.S. (2015) Ribonucleotide reductase and cancer:
595 biological mechanisms and targeted therapies. *Oncogene*, **34**, 2011–2021.

596 18. Greene,B.L., Kang,G., Cui,C., Bennati,M., Nocera,D.G., Drennan,C.L. and Stubbe,J. (2020)
597 Ribonucleotide Reductases (RNRs): Structure, chemistry, and metabolism suggest new
598 therapeutic targets. *Annu Rev Biochem*, **89**, 45–75.

599 19. Bangru,S., Arif,W., Seimetz,J., Bhate,A., Chen,J., Rashan,E.H., Carstens,R.P., Anakk,S. and
600 Kalsotra,A. (2018) Alternative Splicing Rewires Hippo Signaling Pathway in Hepatocytes to
601 Promote Liver Regeneration. *Nat Struct Mol Biol*, **25**, 928–939.

602 20. Choi,H.-S., Chung,M., Tzameli,I., Simha,D., Lee,Y.-K., Seol,W. and Moore,D.D. (1997)
603 Differential Transactivation by Two Isoforms of the Orphan Nuclear Hormone Receptor
604 CAR*. *Journal of Biological Chemistry*, **272**, 23565–23571.

605 21. Forman,B.M., Tzameli,I., Choi,H.-S., Chen,J., Simha,D., Seol,W., Evans,R.M. and
606 Moore,D.D. (1998) Androstane metabolites bind to and deactivate the nuclear receptor CAR-
607 β. *Nature*, **395**, 612–615.

608 22. Wheeler,L.J. and Mathews,C.K. (2011) Nucleoside Triphosphate Pool Asymmetry in
609 Mammalian Mitochondria. *J Biol Chem*, **286**, 16992–16996.

610 23. Keene,K.L., Quinlan,A.R., Hou,X., Hall,I.M., Mychaleckyj,J.C., Onengut-Gumuscu,S. and
611 Concannon,P. (2012) Evidence for two independent associations with type 1 diabetes at the
612 12q13 locus. *Genes Immun*, **13**, 66–70.

613 24. Niu,B., Coslo,D.M., Bataille,A.R., Albert,I., Pugh,B.F. and Omiecinski,C.J. (2018) In vivo
614 genome-wide binding interactions of mouse and human constitutive androstane receptors
615 reveal novel gene targets. *Nucleic Acids Res*, **46**, 8385–8403.

616 25. Cheng,S.L., Bammler,T.K. and Cui,J.Y. (2017) RNA Sequencing Reveals Age and Species
617 Differences of Constitutive Androstane Receptor–Targeted Drug-Processing Genes in the
618 Liver. *Drug Metab Dispos*, **45**, 867–882.

619 26. Moreno,E., Matondo,A.B., Bongiovanni,L., van de Lest,C.H.A., Molenaar,M.R.,
620 Toussaint,M.J.M., van Essen,S.C., Houweling,M., Helms,J.B., Westendorp,B., *et al.* (2022)
621 Inhibition of polyploidization in Pten-deficient livers reduces steatosis. *Liver Int*, **42**, 2442–
622 2452.

623 27. Yang,H. and Wang,H. (2014) Signaling control of the constitutive androstane receptor
624 (CAR). *Protein Cell*, **5**, 113–123.

625 28. Mäkinen,J., Frank,C., Jyrkkärinne,J., Gynther,J., Carlberg,C. and Honkakoski,P. (2002)
626 Modulation of Mouse and Human Phenobarbital-Responsive Enhancer Module by Nuclear
627 Receptors. *Mol Pharmacol*, **62**, 366–378.

628 29. Goldenson,B. and Crispino,J.D. (2015) The Aurora Kinases in Cell Cycle and Leukemia.
629 *Oncogene*, **34**, 537–545.

630 30. Tanaka,H., Arakawa,H., Yamaguchi,T., Shiraishi,K., Fukuda,S., Matsui,K., Takei,Y. and
631 Nakamura,Y. (2000) A ribonucleotide reductase gene involved in a p53-dependent cell-cycle
632 checkpoint for DNA damage. *Nature*, **404**, 42–49.

633 31. Buchanan,J.M. and Hartman,S.C. (1959) Enzymic Reactions in the Synthesis of the Purines.
634 In *Advances in Enzymology and Related Areas of Molecular Biology*. John Wiley & Sons, Ltd,
635 pp. 199–261.

636 32. Rayl,E.A., Moroson,B.A. and Beardsley,G.P. (1996) The Human *pur*H Gene Product, 5-
637 Aminoimidazole-4-carboxamide Ribonucleotide Formyltransferase/IMP Cyclohydrolase.
638 *Journal of Biological Chemistry*, **271**, 2225–2233.

639 33. Reichard,P. (1988) Interactions between deoxyribonucleotide and DNA synthesis. *Annual*
640 *Review of Biochemistry*, **57**, 349–374.

641 34. Song,S., Pursell,Z.F., Copeland,W.C., Longley,M.J., Kunkel,T.A. and Mathews,C.K. (2005)
642 DNA precursor asymmetries in mammalian tissue mitochondria and possible contribution to
643 mutagenesis through reduced replication fidelity. *Proc Natl Acad Sci U S A*, **102**, 4990–4995.

644 35. Greene,B.L., Nocera,D.G. and Stubbe,J. (2018) Basis of dATP inhibition of RNRs. *J Biol*
645 *Chem*, **293**, 10413–10414.

646 36. Ando,N., Li,H., Brignole,E.J., Thompson,S., McLaughlin,M.I., Page,J.E., Asturias,F.J.,
647 Stubbe,J. and Drennan,C.L. (2016) Allosteric Inhibition of Human Ribonucleotide Reductase
648 by dATP Entails the Stabilization of a Hexamer. *Biochemistry*, **55**, 373–381.

649 37. Elledge,S.J., Zhou,Z. and Allen,J.B. (1992) Ribonucleotide reductase: regulation, regulation,
650 regulation. *Trends in Biochemical Sciences*, **17**, 119–123.

651 38. Stamatiou,K., Huguet,F., Serapinas,L.V., Spanos,C., Rappsilber,J. and Vagnarelli,P. (2024)
652 Ki-67 is necessary during DNA replication for fork protection and genome stability. *Genome*
653 *Biology*, **25**, 105.

654 39. Tsai,Y.-F., Fang,M.-C., Chen,C.-H., Yu,I.-S., Shun,C.-T., Tao,M.-H., Sun,C.-P., Lu,J.,
655 Sheu,J.-C., Hsu,Y.-C., *et al.* (2024) Enhancement of adult liver regeneration in mice through
656 the hepsin-mediated epidermal growth factor receptor signaling pathway. *Commun Biol*, **7**,
657 1672.

658 40. Schönenberger,F., Deutzmann,A., Ferrando-May,E. and Merhof,D. (2015) Discrimination of
659 cell cycle phases in PCNA-immunolabeled cells. *BMC Bioinformatics*, **16**, 180.

660 41. Donne R, Saroul-Aïnama M, Cordier P, Celton-Morizur S, Desdouets C. (2020) Polyploidy
661 in liver development, homeostasis and disease. *Nat Rev Gastroenterol Hepatol*, **17**, 391-405.

662 42. Hristova,D., Wu,C.-H., Jiang,W., Krebs,C. and Stubbe,J. (2008) Importance of the
663 Maintenance Pathway in the Regulation of the Activity of Escherichia coli Ribonucleotide
664 Reductase. *Biochemistry*, **47**, 3989–3999.

665 43. Aye,Y., Long,M.J.C. and Stubbe,J. (2012) Mechanistic Studies of Semicarbazone Triapine
666 Targeting Human Ribonucleotide Reductase in Vitro and in Mammalian Cells. *J Biol Chem*,
667 **287**, 35768–35778.

668 44. Dong,B., Lee,J.-S., Park,Y.-Y., Yang,F., Xu,G., Huang,W., Finegold,M.J. and Moore,D.D.
669 (2015) Activating CAR and β-catenin induces uncontrolled liver growth and tumorigenesis.
670 *Nature Communications*, **6**, 5944.

671 45. Zhang,S., Zhou,K., Luo,X., Li,L., Tu,H.-C., Sehgal,A., Nguyen,L.H., Zhang,Y., Gopal,P.,
672 Tarlow,B.D., *et al.* (2018) The Polyploid State Plays a Tumor-Suppressive Role in the Liver.
673 *Developmental Cell*, **47**, 390.

674